주기적인 구형격자로 로딩된 유전체 코팅된 도체 실린더의 복사 특성

Radiation Characteristics of Dielectric-Coated Conducting Cylinder Loaded with Periodic Corrugation

김중표* · 손 현

Joong-Pyo Kim* · Hyon Son

요 약

주기적인 구형격자를 갖는 유전체 코팅된 도체 실린더에 대해 무한 주기 구조와 유한 주기 구조에 대한 누설파 안테나의 복사 특성을 이론적으로 해석하였다. 무한 주기 구조에 대하여는 모드 정합 법을 적용하여 해석하였고, 유한 주기 구조에 대하여는 퓨리에 변환과 모드 전개를 사용하여 적분 방정식을 유도하고 선형 연립 방정식을 얻는다. 구형격자의 폭, 깊이, 유전체 코팅두께, 도체 실린더의 반경, 유한 구형격자 개수의 영향이 위상 상수, 누설 상수 및 복사패턴 등과 복사 특성에 미치는 영향을 조사하였고, 유한 주기 구조와 무한 주기 구조의 결과를 비교하고 잘 일치함을 확인할 수 있었다. 균일 유한 주기 구형격자에 의한 높은 측엽을 줄이기 위해 안테나의 전후단 부에 테이퍼링과 비균일 준주기 슬롯배열을 고려하였다. 또한 구형격자 표면파 안테나에 사용되는 구형격자 주기, 폭, 깊이에 대해 테이퍼링을 통해 낮은 측엽을 갖는 endfire 복사패턴을 얻을 수 있었다.

Abstract

The radiation characteristics of leaky wave antenna from the dielectric-coated conducting cylinder with periodic corrugation are investigated theoretically for the infinite and finite periodic structures. For the infinite periodic structure, mode-matching method is applied. The integral equation is derived for the finite periodic structure by use of the Fourier transform and mode expansion and a simultaneous linear equation is obtained. The influences of the corrugation slot width, corrugation depth, dielectric thickness, cylinder radius, and finite corrugation number on the radiation characteristics (leakage constant, phase constant, and radiation pattern) are investigated. The results of the finite periodic corrugations are compared with those of the infinite extent structure and good agreement is found. To reduce high side lobe levels of the uniform finite periodic structure, tapering process on the beginning and end section of antenna and nonuniform quasi-period slot arrays are considered. Especially, for the corrugation period, width and depth used for a corrugated surface wave antenna, through the proper tapering process, end-fire radiation pattern with reduced side lobe levels is given.

I. Introduction

Periodic open guiding structures are known to be the main components of various microwave and millimeterwave devices and circuits(Bragg reflection filter, leaky wave antenna, etc). In particular,

경북대학교 전자공학과(Department of Electronics, Kyungpook National University)
* 한국항공우주연구소(Korea Aerospace Research Institute)
· 논 문 번 호 : 991023-094
· 수정완료일자 : 1999년 12월 3일

radiating dielectric-based structures transforming guided modes to free space waves play a large role in most applications of microwaves and millimeter-waves. Their attractiveness lies in simplicity of fabrication, relatively low cost factor, planar construction, and frequency scanning ability. Owing to promising applications, the basic physical phenomenon of directional radiation of a leaky wave travelling along a periodically loaded infinite waveguide is under active study at present[1]~[7].

Until now, problems for the periodic open guiding structure of planar type has been extensively investigated, those for the periodic open guiding structure of cylinder type only have a few. Recently, a circular dielectric waveguide with periodic corrugations and a metallic grating loaded circular dielectric waveguide were investigated theoretically and experimentally to produce an omnidirectional leaky wave antenna[8],[9]. Also a dielectric-coated coaxial waveguide periodic slot with finite and zero thickness was proposed and analyzed to obtain a simpler feeding structure and improve the performance of leaky wave antennas[10].

In this paper, a new omnidirectional leaky wave and surface wave antenna is proposed and analyzed. That is finite periodic corrugation loaded dielectric-coated conducting cylinder. The mode matching technique is applied to the analysis of an infinite periodic corrugation structure, In the mode matching formulation, the radial waveguide mode is employed to express the fields in the corrugation region, and space harmonics in other regions. Boundary conditions are imposed at the interfaces and a homogeneous linear equation is obtained. The phase and leakage constants which determine the radiation characteristics of a leaky wave *antenna are calculated by the nontrivial condition* of the homogeneous linear equation.

To find the effect of the feeding and finite length of the structure, a resolution method for the *finite periodic* structure is needed. For this case, fields in the corrugation regions are expressed as summation of the radial waveguide TM modes, which is similar to the infinite structure, and in other regions are expressed in the spectral domain by using the inverse Fourier transformation. Boundary conditions at the interfaces are enforced, and the simultaneous linear equations are derived.

The influences of the corrugation slot width, corrugation depth, dielectric thickness, and cylinder radius on the radiation characteristics(leakage constant, phase constant, and radiation pattern) are investigated. The effects of the corrugation number are also studied by increasing the total corrugation number. The results of the finite periodic corrugations are compared with those of the infinite extent structure and good agreement has been found. It has been observed that when the leaky wave mode is established in the finite structure, most of incident power is radiated into free space.

The uniform finite periodic corrugation has relatively high side lobes. For reduced side lobes and narrow beam requirements, through tapering process of the beginning and end section of the antennas, we obtained the radiation pattern with reduced side lobes. Also to accomplish that the minimum main beam width at given side lobe level have to be reached, we synthesized Taylor pattern to produce the desired radiation pattern[12].

Especially, the corrugation finite periodic structure gives end-fire radiation pattern with specified corrugation period and depth, which was used in a corrugated surface wave antenna[13], but it has very high side lobe levels. Through the proper tapering process, we can obtain end-fire radiation pattern with reduced side lobe levels.

Ⅲ. Formulation for infinite periodic corrugation

The geometry of the problem is circular

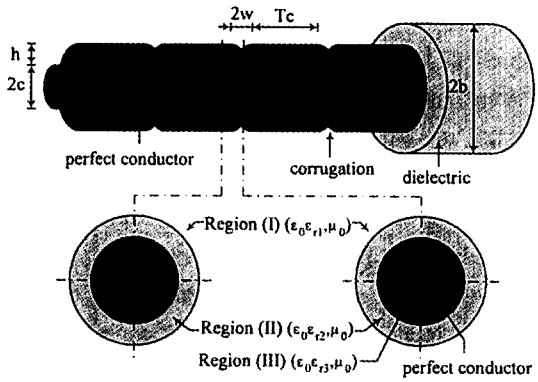

Fig. 1. Geometry of the dielectric coated conducting cylinder loaded with corrugation.

symmetry and it is assumed that the magnetic field has only ϕ component(TM case). For the periodic structure shown in Fig. 1, the fields in each region are expressed in a different way. In region (I), the fields are expressed as a summation of space harmonics and outgoing waves in the ρ-direction by

$$H_\phi^{(I)}(\rho,z) = \sum_{n=-\infty}^{\infty} C_n H_1^{(2)}(k_{\rho n}^{(1)}\rho)e^{-jk_{zn}z},$$

$$E_z^{(I)}(\rho,z) = \frac{1}{j\omega\varepsilon_0\varepsilon_{r1}} \sum_{n=-\infty}^{\infty} C_n k_{\rho n}^{(1)} H_0^{(2)} \cdot (k_{\rho n}^{(1)}\rho)e^{-jk_{zn}z}, \quad (1)$$

where $k_{\rho n}^{(1)} = \sqrt{\varepsilon_{r1}k_0^2 - k_{zn}^2}$, $k_{zn} = k_{z0} + 2n\pi/T_c$, and $k_{z0} = \beta - j\alpha$. $H_n^{(2)}(\cdot)$ is the n-th order Hankel function of the second kind and C_n are the unknown complex amplitudes of the space harmonics, and k_{zn} is complex propagation constant which must be determined. In region (II), the fields are expressed as a summation of space harmonics and standing waves in the ρ-direction by

$$H_\phi^{(II)}(\rho,z) = \sum_{n=-\infty}^{\infty} [D_n H_1^{(1)}(k_{\rho n}\rho^{(2)}) + D_n' H_1^{(2)}(k_{\rho n}^{(2)}\rho)]e^{-jk_{zn}z},$$

$$E_z^{(II)}(\rho,z) = \frac{1}{j\omega\varepsilon_0\varepsilon_{r2}} \sum_{n=-\infty}^{\infty} k_{\rho n}^{(2)} \cdot [D_n H_0^{(1)}(k_{\rho n}^{(2)}\rho) + D_n' H_0^{(2)}(k_{\rho n}^{(2)}\rho)]e^{-jk_{zn}z}, \quad (2)$$

where $k_{\rho n}^{(2)} = \sqrt{\varepsilon_{r2}k_0^2 - k_{zn}^2}$.

In region (III), the fields are expressed as a superposition of the radial waveguide modes,

$$H_\phi^{(III)}(\rho,z) = \sum_{m=0}^{\infty} [B_m H_1^{(1)}(k_{\rho m}^{(3)}\rho) + B_m H_1^{(2)}(k_{\rho m}^{(3)}\rho)]\cos\frac{m\pi}{2w}(z+w),$$

$$E_z^{(III)}(\rho,z) = \frac{1}{j\omega\varepsilon_0\varepsilon_{r3}} \sum_{m=0}^{\infty} k_{\rho m}^{(3)} \cdot [B_m H_0^{(1)}(k_{\rho m}^{(3)}\rho) + B_m' H_0^{(2)}(k_{\rho m}^{(3)}\rho)] \cdot \cos\frac{m\pi}{2w}(z+w), \quad (3)$$

where $k_{\rho m}^{(3)} = \sqrt{\varepsilon_{r3}k_0^2 - (m\pi/2w)^2}$, B_m and B_{m6}' are the unknown complex amplitudes of radial waveguide modes.

The continuity condition of the tangential electric and magnetic fields is imposed at the interfaces $\rho = a$ for $|z| \le w$ and $\rho = b$ for $|z| \le T_c/2$ and the tangential electric field is enforced to be zero on the conductor surfaces. The resulting equations for the electric field are multiplied by the space harmonic functions and integrated over the period. The equations for the magnetic field are multiplied by radial waveguide modes and integrated over the slot. After considering the orthogonality properties of modes and space harmonics, the following matrix equations are obtained:

$$\boldsymbol{SD'} = \boldsymbol{B}, \quad (4)$$

$$\boldsymbol{D'} = \boldsymbol{RB}, \quad (5)$$

where

$$S_{mn} = [R_n^h H_1^{(1)}(k_{\rho n}^{(2)}a) + H_1^{(2)}(k_{\rho n}^{(2)}a)] \cdot \frac{H_0^{(2)}(k_{\rho m}^{(3)}c)H_0^{(1)}(k_{\rho m}^{(3)}a)}{H_0^{(2)}(k_{\rho m}^{(3)}c)H_1^{(1)}(k_{\rho m}^{(3)}a) - H_0^{(1)}(k_{\rho m}^{(3)}c)H_1^{(2)}(k_{\rho m}^{(3)}a)} \cdot \frac{v_{nm}}{(1+\delta_{m0})w},$$

$$R_{nm} = \frac{\varepsilon_{r2}k_{\rho m}^{(3)}}{T_c\varepsilon_{r3}k_{\rho n}^{(2)}} \cdot$$

$$\frac{1}{R_n^h H_0^{(1)}(k_{\rho n}^{(2)} a) + H_0^{(2)}(k_{\rho n}^{(2)} a)} \cdot$$

$$\frac{H_0^{(2)}(k_{\rho m}^{(3)} c) H_1^{(1)}(k_{\rho m}^{(3)} a) - H_0^{(1)}(k_{\rho m}^{(3)} c) H_1^{(2)}(k_{\rho m}^{(3)} a)}{H_0^{(2)}(k_{\rho m}^{(3)} c) H_0^{(1)}(k_{\rho m}^{(3)} a)}$$

$$\cdot v_{mn}^*,$$

$$v_{mn} = -jk_{zn} \frac{(-1)^m e^{-jk_{zn}w} - a^{jk_{zn}w}}{k_{zn}^2 - (m\pi/2w)^2},$$

and * denotes the complex conjugate. After combining (4) and (5), the following homogeneous matrix equation is obtained

$$[\boldsymbol{I} - \boldsymbol{SR}]\boldsymbol{B} = \boldsymbol{0}, \tag{6}$$

where $\boldsymbol{I}$ is the identity matrix. For a nontrivial solution, the determinant of (6) must be zero. From this condition, the unknown complex propagation constant ($\beta - j\alpha$) is calculated. Once $\beta - j\alpha$ is known, the column matrices $\boldsymbol{B}$, $\boldsymbol{C}$, $\boldsymbol{D}$, and $\boldsymbol{D}'$ are obtained by normalization of fundamental mode B_0. The fields in any region are computed by (1)~(3). The far-field radiation pattern can be calculated from the known tangential electric fields over each corrugation slot by using the equivalence principle. The far-zone magnetic field radiated from a finite section of the infinite structure is given by,

$$H_\phi(R, \theta) \approx \frac{-2w\varepsilon_{r1}}{\pi\varepsilon_{r2}} \sum_{n=-\infty}^{\infty} k_{\rho n}^{(2)} \cdot$$

$$[D_n H_0^{(1)}(k_{\rho n}^{(2)} a) + D'_n H_0^{(2)}(k_{\rho n}^{(2)} a)] \cdot$$

$$F(k_1 \cos\theta) \frac{e^{-jk_1 R}}{R}, \tag{7}$$

where

$$F(\zeta) = \frac{T(\zeta)}{k_{\rho 2}[H_0^{(2)}(k_{\rho 2} a) + R(\zeta) H_0^{(1)}(k_{\rho 2} a)]}$$

$$\cdot \frac{\sin(k_{zn} - \zeta)w}{(k_{zn} - \zeta)w} \frac{1 - e^{-j(k_{zn} - \zeta)MT_c}}{1 - e^{-j(k_{zn} - \zeta)T_c}},$$

$$R(\zeta) = \frac{\varepsilon_{r1} k_{\rho 2} H_0^{(2)}(k_{\rho 2} b) H_1^{(2)}(k_{\rho 1} b)) -}{\varepsilon_{r1} k_{\rho 2} H_0^{(1)}(k_{\rho 2} b) H_1^{(2)}(k_{\rho 1} b) -}$$

$$\frac{\varepsilon_{r2} k_{\rho 1} H_1^{(2)}(k_{\rho 2} b) H_0^{(2)}(k_{\rho 1} b)}{\varepsilon_{r2} k_{\rho 1} H_1^{(1)}(k_{\rho 2} b) H_0^{(2)}(k_{\rho 1} b)},$$

$$T(\zeta) = \frac{\varepsilon_{r1} 4j/(\pi b)}{\varepsilon_{r1} k_{\rho 2} H_0^{(1)}(k_{\rho 2} b) H_1^{(2)}(k_{\rho 1} b) -}$$

$$\frac{}{\varepsilon_{r2} k_{\rho 1} H_1^{(1)}(k_{\rho 2} b) H_0^{(2)}(k_{\rho 1} b)},$$

$$k_{\rho 1} = \sqrt{\varepsilon_{r1} k_0^2 - \zeta^2}, \quad k_{\rho 2} = \sqrt{\varepsilon_{r2} k_0^2 - \zeta^2}$$

and M is the total corrugation slot number taken into account in a finite section of the infinite periodic structure.

Ⅱ. Formulation for finite periodic corrugation

The geometry of dielectric-coated conducting cylinder loaded with finite periodic corrugations is shown in Fig. 2. We suppose that the corrugation is excited by the dominant TM-mode of slab. In region (I), the incident surface waves are expressed as

$$H_\phi^{i(I)}(\rho, z) = K_1(u_1 \rho) e^{-j\lambda z},$$

$$E_z^{i(I)}(\rho, z) = \frac{1}{jw\varepsilon_0\varepsilon_{r1}} u_1 K_0(u_1 \rho) e^{-j\lambda z}, \tag{8}$$

where $u_1 = \sqrt{\lambda^2 - k^2}$ and $K_n(\cdot)$ is the modified Bessel function of the second kind. The scattered fields in region (I) are expressed as a superposition of outgoing waves in ρ direction, by use of the inverse Fourier transform,

$$H_\phi^{s(I)}(\rho, z) = \frac{1}{2\pi} \int_{-\infty}^{\infty} \tilde{H}_\phi^{s(II)}(\zeta) \cdot$$

$$T(\zeta) H_1^{(2)}(k_{\rho 1}\rho) e^{-j\zeta z},$$

$$E_z^{s(I)}(\rho, z) = \frac{1}{2\pi j\omega\varepsilon_0\varepsilon_{r1}} \int_{-\infty}^{\infty} \tilde{H}_\phi^{s(II)}(\zeta),$$

$$T(\zeta) k_{\rho 1} H_0^{(2)}(k_{\rho 1}\rho) e^{-j\zeta z}, \tag{9}$$

where $k_{\rho 1} = \sqrt{k_1^2 - \zeta^2}$. In region (II), the incident surface waves are expressed as

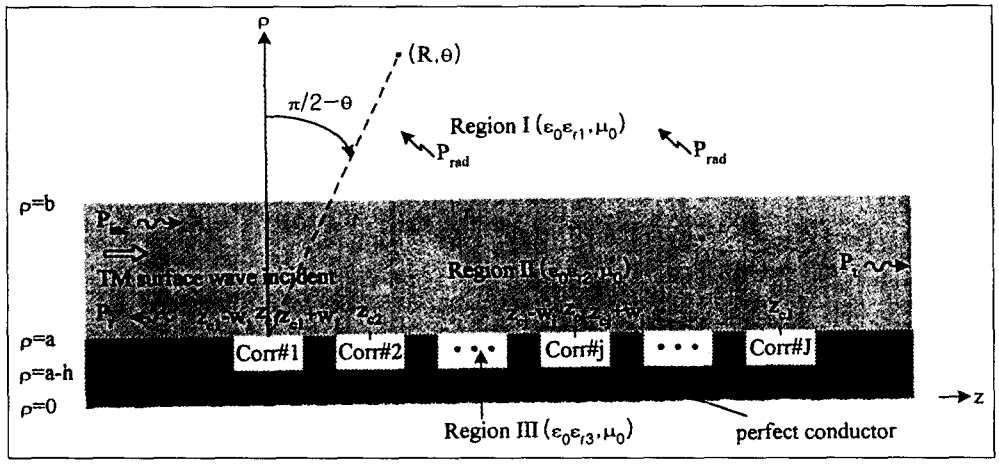

Fig. 2. The geometry of dielectric coated conducting cylinder loaded with finite periodic corrugations.

$$H_\phi^{i(II)}(\rho, z) = K_1(u_1 b)\cdot \frac{J_0(u_2 a)Y_1(u_2\rho) - Y_0(u_2 a)J_1(u_2\rho)}{J_0(u_2 a)Y_1(u_2 b) - Y_0(u_2 a)J_1(u_2 b)} e^{-j\lambda z},$$

$$E_z^{i(II)}(\rho, z) = \frac{1}{j\omega\varepsilon_0\varepsilon_{r2}} u_2 K_1(u_1 b)\cdot \frac{J_0(u_2 a)Y_0(u_2\rho) - Y_0(u_2 a)J_0(u_2\rho)}{J_0(u_2 a)Y_1(u_2 b) - Y_0(u_2 a)J_1(u_2 b)} e^{-j\lambda z}, \quad (10)$$

where $u_2 = \sqrt{\lambda^2 - k_2^2}$. The scattered fields in region (II) are expressed as a superposition of standing waves in the ρ direction,

$$H_\phi^{s(II)}(\rho, z) = \frac{1}{2\pi}\int_{-\infty}^{\infty} \tilde{H}_\phi^{s(II)}(\zeta)\cdot [H_1^{(2)}(k_{\rho 2}\rho) + R(\zeta)H_1^{(1)}(k_{\rho 2}\rho)]e^{-j\zeta z},$$

$$E_z^{s(II)}(\rho, z) = \frac{1}{2\pi j\omega\varepsilon_0\varepsilon_{r2}}\int_{-\infty}^{\infty} \tilde{H}_\phi^{s(II)}(\zeta) k_{\rho 2}\cdot [H_0^{(2)}(k_{\rho 2}\rho) + R(\zeta)H_0^{(1)}(k_{\rho 2}\rho)]e^{-j\zeta z}, \quad (11)$$

where $k_{\rho 2} = \sqrt{k_2^2 - \zeta^2}$. In region (III), the fields in the l-th corrugation slot region are expressed as a summation of radial waveguide TM modes,

$$H_\phi^{(III)}(\rho, z) = \sum_{m=0}^{\infty} C_m^l \cos w_m^l(z + w_l - z_{cl}) \cdot \left[\frac{H_0^{(2)}(k_{\rho 3m}^l c)H_1^{(1)}(k_{\rho 3m}^l \rho)}{H_0^{(2)}(k_{\rho 3m}^l c)H_0^{(1)}(k_{\rho 3m}^l a)} - \frac{H_0^{(1)}(k_{\rho 3m}^l c)H_1^{(2)}(k_{\rho 3m}^l \rho)}{H_0^{(2)}(k_{\rho 3m}^l c)H_0^{(1)}(k_{\rho 3m}^l a)}\right], \quad (12)$$

$$E_z^{(III)}(\rho, z) = \frac{1}{j\omega\varepsilon_0\varepsilon_{r3}}\sum_{m=0}^{\infty} C_m^l \cdot \cos w_m^l(z + w_l - z_{cl}) k_{\rho 3m}^l \cdot \left[\frac{H_0^{(2)}(k_{\rho 3m}^l c)H_0^{(1)}(k_{\rho 3m}^l \rho)}{H_0^{(2)}(k_{\rho 3m}^l c)H_0^{(1)}(k_{\rho 3m}^l a)} - \frac{H_0^{(1)}(k_{\rho 3m}^l c)H_0^{(2)}(k_{\rho 3m}^l \rho)}{H_0^{(2)}(k_{\rho 3m}^l c)H_0^{(1)}(k_{\rho 3m}^l a)}\right], \quad (12)$$

where $k_{\rho 3m}^l = \sqrt{k_3^2 - w_m^{l^2}}$ and $w_m^l = m\pi/2w_l$.

The tangential fields continuities at $\rho = b$ are already satisfied by introducing $R(\zeta)$ and $T(\zeta)$. The tangential electric field continuity at $\rho = a$ yields

$$\tilde{H}_\phi^{s(II)}(\zeta) = \frac{\varepsilon_{r2}}{\varepsilon_{r3} k_{\rho 2} M_e(\zeta)} \cdot \sum_{l=1}^{L}\sum_{m=0}^{\infty} C_m^l k_{\rho 3m}^l \Omega_m^l P_m^l(\zeta) \quad (13)$$

where

$$M_e(\zeta) = H_0^{(2)}(k_{\rho 2} a) + R(\zeta)H_0^{(1)}(k_{\rho 2} a),$$

$$\Omega^l_{e,m}=\left[\frac{H_0^{(2)}(k^l_{\rho 3m}c)H_0^{(1)}(k^l_{\rho 3m}a)}{H_0^{(2)}(k^l_{\rho 3m}c)H_0^{(1)}(k^l_{\rho 3m}a)}-\frac{H_0^{(1)}(k^l_{\rho 3m}c)H_0^{(2)}(k^l_{\rho 3m}a)}{H_0^{(2)}(k^l_{\rho 3m}c)H_0^{(1)}(k^l_{\rho 3m}a)}\right]$$

$$P^l_m(\zeta)=\frac{-j\zeta[(-1)^m e^{j\zeta w_l}-e^{-j\zeta w_l}]e^{j\zeta z_{cl}}}{\zeta^2-w_m^{l\,2}}$$

The tangential magnetic field continuity on the aperture of the corrugations at $\rho=a$ and the use of mode orthogonality give

$$\sum_{l=1}^{J}\sum_{m=0}^{\infty}C^l_m k^l_{\rho 3m}\Omega^l_{e,m}\frac{\varepsilon_{r2}}{2\pi\varepsilon_{r3}}K^{rl}_{nm}-C^r_n\Omega^l_{h,m}\alpha_n w_r=-R^h_\lambda p^r_n(-\lambda), \qquad (14)$$

where

$$K^{rl}_{nm}=\int_{-\infty}^{\infty}\frac{M_h(\zeta)}{k_{\rho 2}M_e(\zeta)}P^l_m(\zeta)P^r_n(-\zeta)d\zeta,$$

$$M_h(\zeta)=H_1^{(2)}(k_{\rho 2}a)+R(\zeta)H_1^{(1)}(k_{\rho 2}a)$$

$$\Omega^l_{e,m}=\left[\frac{H_0^{(2)}(k^l_{\rho 3m}c)H_1^{(1)}(k^l_{\rho 3m}a)}{H_0^{(2)}(k^l_{\rho 3m}c)H_0^{(1)}(k^l_{\rho 3m}a)}-\frac{H_0^{(1)}(k^l_{\rho 3m}c)H_1^{(2)}(k^l_{\rho 3m}a)}{H_0^{(2)}(k^l_{\rho 3m}c)H_0^{(1)}(k^l_{\rho 3m}a)}\right].$$

and $\alpha_n=2$, for $n=0$, $\alpha_n=1$ for $n\neq 0$. Since the integrand of K^{rl}_{nm} contains the surface wave poles and branch points, the integrand path can be deformed into a path along the branch cut[10]. The reason for this path deformation is to obtain a faster convergent integral. The integral path deformation gives

$$K^{rl}_{nm}=2\pi w_l\eta_{Km}\delta_{nm}\delta_{rl}+L^{rl}_{nm}, \qquad (15)$$

where

$$\eta_{Km}=\begin{cases}0, & w^l_m<k_1\\ \left.\dfrac{M_h(\zeta)}{k_{\rho 2}M_e(\zeta)}\right|_{\zeta=w^l_m}, & \text{elsewhere}\end{cases}$$

$$L^{rl}_{nm}=-2\pi j\sum_q Q^{rl}_{q,nm}+L^{rl}_{nm},$$

$$Q^{rl}_{q,nm}=\begin{cases}0, & l=r,\ m+n=\text{odd}\\ G(\lambda_q)\dfrac{2\lambda_q^2[1-(-1)^m\cos 2\lambda_q w_l]}{(\lambda_q-w^l_m)^2(\lambda_q+w^l_m)^2}, & l=r,\ m+n,\ w^l_m<k_1\\ G(\lambda_q)\dfrac{2\lambda_q^2[1-(-1)^m e^{-2\lambda_q w_l}]}{(\lambda_q-w^l_m)(\lambda_q^2-w^{r2}_n)}, & l=r,\ m+n=\text{even},\ w^l_m>k_1\\ G(\lambda_q^2)\dfrac{2\lambda_q^2 h(\lambda_q)}{(\lambda_q^2-w^l_m)(\lambda_q^2-w^{r2}_n)}, & l\neq r\end{cases}$$

$$Q^{rl}_{q,nm}=\begin{cases}0, & l=r,\ m+n=\text{odd}\\ R_1, & l=r,\ m=n,\ w^l_m<k_1\\ R_2+R'_2, & l=r,\ m+n=\text{even},\ w^l_m>k_1\\ R_3+R'_3, & l\neq r\end{cases}$$

$$G(\lambda_q)=\lim_{\zeta\to\lambda_q}(\zeta-\lambda_q)\frac{M_h(\zeta)}{k_{\rho 2}M_e(\zeta)}$$

$$R_1=PV\int_0^\infty\frac{M_h(\zeta)}{k_{\rho 2}M_e(\zeta)}\cdot\frac{2\zeta^2[1-(-1)^m\cos 2\zeta w_l]}{(\zeta-w^l_m)^2(\zeta+w^l_m)^2}d\zeta$$

$$R_2=\frac{2j}{h}\int_0^\infty \mathrm{Im}\left\{\left.\frac{M_h(\zeta)}{k_{\rho 2}M_e(\zeta)}\right|_{\substack{k_{\rho 1}=s_1\\ k_{\rho 2}=s_2\\ \zeta=-j\alpha/h}}\right\}\cdot\frac{-2(\alpha/h)^2[1-(-1)^m e^{-2\alpha/hw_l}]}{[(\alpha/h)^2+w^{l2}_m][(\alpha/h)^2+w^{r2}_n]}d\alpha$$

$$R'_2=\frac{2}{h}\int_0^{k_1 h}\mathrm{Im}\left\{\left.\frac{M_h(\zeta)}{k_{\rho 2}M_e(\zeta)}\right|_{\substack{k_{\rho 1}=q_1\\ k_{\rho 2}=q_2\\ \zeta=\beta/h}}\right\}\cdot\frac{2(\beta/h)^2[1-(-1)^m e^{-2\beta/hw_l}]}{[(\beta/h)^2-w^{l2}_m][(\beta/h)^2-w^{r2}_n]}d\beta$$

$$R_3=\frac{2j}{h}\int_0^\infty \mathrm{Im}\left\{\left.\frac{M_h(\zeta)}{k_{\rho 2}M_e(\zeta)}\right|_{\substack{k_{\rho 1}=s_1\\ k_{\rho 2}=s_2\\ \zeta=-j\alpha/h}}\right\}\cdot\frac{-(\alpha/h)^2 h(-j\alpha/h)}{[(\alpha/h)^2+w^{l2}_m][(\alpha/h)^2+w^{r2}_n]}d\alpha$$

$$R'_3 = \frac{2}{h}\int_0^{k_1 h} \mathrm{Im}\left\{ \frac{M_h(\zeta)}{k_{\rho 2} M_e(\zeta)}\Big|_{\substack{k_{\rho 1}=q_1 \\ k_{\rho 2}=q_2 \\ \zeta=\beta/h}} \right\} \cdot \frac{(\beta/h)^2 h(\beta/h)}{[(\beta/h)^2 - w_m^{r2}][(\beta/h)^2 - w_n^{r2}]}\, d\beta$$

$$h(\zeta) = (-1)^{m+n} e^{-j\zeta|z_{cl}-z_{cr}+w_l-w_r|} + e^{-j\zeta|z_{cl}-z_{cr}-w_l+w_r|} - (-1)^m e^{-j\zeta|z_{cl}-z_{cr}+w_l+w_r|} - (-1)^n e^{-j\zeta|z_{cl}-z_{cr}-w_l-w_r|},$$

$$s_1 = \sqrt{k_1^2+(\alpha/h)^2},\quad s_2 = \sqrt{k_2^2+(\alpha/h)^2},$$

$$q_1 = \sqrt{k_1^2-(\beta/h)^2},\quad q_2 = \sqrt{k_2^2-(\beta/h)^2}$$

and λ_q is the solution of $M_e(\zeta)|_{\lambda_q=0}$ which is the well known modal equation for axial surface wave on a dielectric-coated conductor. From (14), we can obtain following simultaneous linear equation:

$$(\phi)(C) = (S) \tag{16}$$

where

$$\psi_{nm}^{rl} = \left[k_{\rho 3m}^l \Omega_{e,m}^l \frac{\varepsilon_{r2}}{\varepsilon_{r3}} w_l \eta_{Km} - \alpha_n w_r \Omega_{h,m}^l \right] \cdot \delta_{nm}\delta_{rl} + k_{\rho 3m}^l \Omega_{e,m}^l \frac{\varepsilon_{r2}}{2\pi\varepsilon_{r3}} L_{nm}^{rl},$$

$$S_n^r = R_\lambda^h P_n^r(-\lambda).$$

Once the unknown radial waveguide mode coefficient C_m^l is determined by solving (16), $\tilde{H}_\phi^{s(II)}(\zeta)$ is computed by (13). Hence, the fields in each region can be calculated by the use of the field equations (9), (11), and (12). The waves scattered by the corrugation are divided into two wave types, i.e., one is the space wave which is radiated into region (I), and the other the surface wave which is trapped in and above the dielectric and guided in the $\pm z$-directions. The far-zone magnetic field radiated into (I), by using an asymptotic evaluation, is given as

$$H_{\phi,space}^{s(I)}(R,\theta) = \sum_{l=1}^{L}\sum_{m=0}^{\infty} C_m^l k_{\rho 3m}^l \cdot \Omega_{e,m}^l \frac{-\varepsilon_{r2}}{\pi\varepsilon_{r3}} F_{space}(k_1\cos\theta)\frac{e^{-jk_1R}}{R}, \tag{17}$$

where

$$F_{space}(\zeta) = \frac{\varepsilon_{r1}k_{\rho 2}[H_1^{(2)}(k_{\rho 2}b)H_0^{(2)}(k_{\rho 2}b) - k_{\rho 2}[M^+(\zeta)H_0^{(2)}(k_{\rho 2}a) - \cdot \frac{H_1^{(1)}(k_{\rho 2}b)H_0^{(1)}(k_{\rho 2}b)]}{M^-(\zeta)H_0^{(1)}(k_{\rho 2}a)]} P_m^l(\zeta),$$

$$M^+(\zeta) = \varepsilon_{r1}k_{\rho 2}H_0^{(1)}(k_{\rho 2}b)H_1^{(2)}(k_{\rho 2}b) - \varepsilon_{r2}k_{\rho 1}H_1^{(1)}(k_{\rho 2}b)H_0^{(2)}(k_{\rho 2}b),$$

$$M^-(\zeta) = \varepsilon_{r1}k_{\rho 2}H_0^{(2)}(k_{\rho 2}b)H_1^{(2)}(k_{\rho 2}b) - \varepsilon_{r2}k_{\rho 1}H_1^{(2)}(k_{\rho 2}b)H_0^{(2)}(k_{\rho 2}b),$$

from which the radiation pattern is calculated. The surface wave in each region is calculated by applying the Cauchy residue theorem on (9) and (11), and is expressed as

$$H_{\phi,surf}^{s(I)\pm}(\rho,z) = \mp j\sum_q \sum_{l=1}^{L}\sum_{m=0}^{\infty} C_m^l k_{\rho 3m}^l \Omega_{e,m}^l \cdot \frac{1}{\varepsilon_{r3}} F_{surf}^{(I)}(\pm\lambda_q) e^{\mp j\lambda_q z},$$

$$H_{\phi,surf}^{s(II)\pm}(\rho,z) = \mp j\sum_q \sum_{l=1}^{L}\sum_{m=0}^{\infty} C_m^l k_{\rho 3m}^l \Omega_{e,m}^l \cdot \frac{\varepsilon_{r2}}{\varepsilon_{r3}} F_{surf}^{(II)}(\pm\lambda_q) e^{\mp j\lambda_q z}, \tag{18}$$

where

$$F_{surf}^{(I)}(\pm\lambda_q) = \lim_{\zeta\to\lambda_q}(\zeta\mp\lambda_q) \cdot \frac{[M^+(\zeta)H_0^{(2)}(k_{\rho 2}b) - k_{\rho 1}H_0^{(2)}(k_{\rho 1}b)[M^+(\zeta)H_0^{(2)}(k_{\rho 2}a) - \frac{M^-(\zeta)H_0^{(1)}(k_{\rho 2}b)]}{M^-(\zeta)H_0^{(1)}(k_{\rho 2}a)]} P_m^l(\zeta)H_1^{(2)}(k_{\rho 2}\rho),$$

$$F_{surf}^{(II)}(\pm\lambda_q) = \lim_{\zeta\to\lambda_q}(\zeta\mp\lambda_q) \cdot \frac{[M^+(\zeta)H_1^{(2)}(k_{\rho 2}\rho) - M^-(\zeta)H_1^{(1)}(k_{\rho 2}\rho)]}{k_{\rho 2}[M^+(\zeta)H_0^{(2)}(k_{\rho 2}a) - M^-(\zeta)H_0^{(1)}(k_{\rho 2}a)]} \cdot P_m^l(\zeta),$$

and the superscript ± means positive and negative z-direction travelling waves, respectively. The time-averaged incident power(P_{inc}), reflected power(P_r), transmitted power(P_t), and radiated power(P_{rad}) are given by

$$P_{inc} = \frac{\pi\eta_0}{2k_0\varepsilon_{r1}}\lambda\{b^2[K_0(u_1 b)]^2 + \frac{2b}{u_1}K_0(u_1 b)K_1(u_1 b) - b^2[K_1(u_1 b)]^2\} + \frac{\pi\eta_0}{2k_0\varepsilon_{r2}}\lambda[K_1(u_1 b)]^2 \left\{ b^2 + b^2\left[\frac{\varepsilon_{r2}u_1K_0(u_1 b)}{\varepsilon_{r1}u_2K_1(u_1 b)}\right]^2 + \frac{2b}{u_1}\frac{\varepsilon_{r2}u_1K_0(u_1 b)}{\varepsilon_{r1}u_2K_1(u_1 b)} - a^2\left[\frac{J_0(u_2 a)Y_1(u_2 a) - Y_0(u_2 a)J_1(u_2 a)}{J_0(u_2 a)Y_1(u_2 b) - Y_0(u_2 a)J_1(u_2 b)}\right]^2 \right\} \quad (19)$$

$$P_r = P_{inc}|\sum_q C(-\lambda_q)|^2, \quad (20)$$

$$P_t = P_{inc}|1 - \sum_q C(-\lambda_q)|^2, \quad (21)$$

$$P_{rad} = \pi\eta_1 \int_o^{\pi} \left| \sum_{l=1}^{I}\sum_{m=0}^{\infty} C^l_m k^l_{\rho 3m}\Omega^l_{e,m} \cdot \frac{-1}{2\pi\varepsilon_{r3}} F_{sapce}(k_1\cos\theta)\right|^2 \sin\theta\, d\theta, \quad (22)$$

where

$$C(\zeta) = j\sum_{l=1}^{I}\sum_{m=0}^{\infty} C^l_m k_{\rho 3m}\Omega^l_{e,m}\frac{\varepsilon_{r2}}{\varepsilon_{r3}}\frac{2}{\pi b} \cdot \frac{1}{u_2\frac{d}{d\zeta}D_{TM}(\zeta)}P^l_m(\zeta),$$

$$D_{TM}(\zeta) = \varepsilon_{r1}u_2K_1(u_1 b)\cdot[J_0(u_2 a)Y_0(u_2 b) - Y_0(u_2 a)J_0(u_2 b)] + \varepsilon_{r2}u_1K_0(u_1 b)\cdot[J_0(u_2 a)Y_1(u_2 b) - Y_0(u_2 a)J_1(u_2 b)].$$

The validity of the numerical results is assured by a check of the power conservation law

$$P_{inc} = P_r + P_t + P_{rad} \quad (23)$$

Ⅳ. Numerical results and discussion

To be certain that the complex propagation constant($\beta - ja$) converges to the correct value, we calculate the tangential electric and magnetic fields at the interfaces(at $\rho = a$ and b) for a

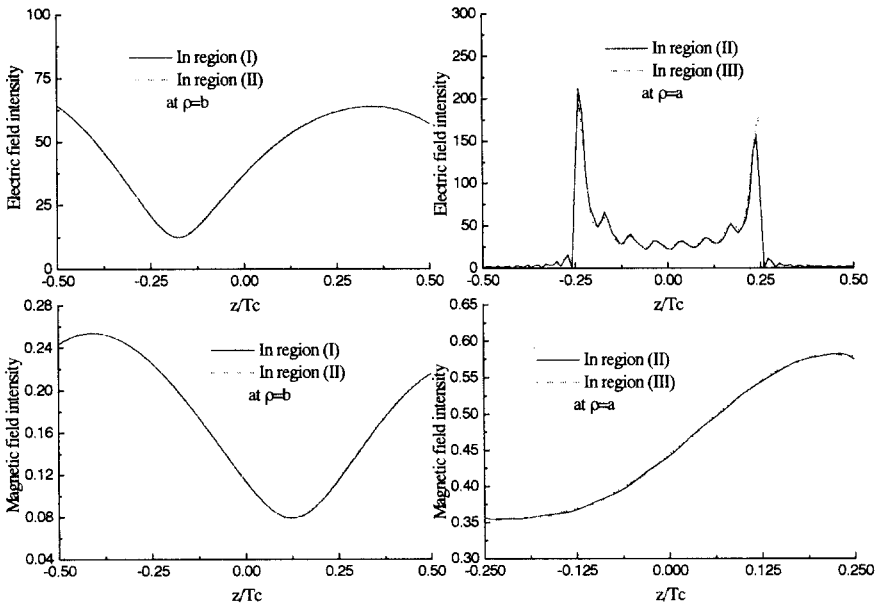

Fig. 3. Field amplitudes at interfaces. a=0.35 λ, b=0.55 λ, h=0.05 λ, T_c=0.6 λ, w=0.25 λ, T_c=0.6 λ, ε_{r1}=1, ε_{r2}=2, ε_{r3}=2.

corrugation structure having $a=0.35\lambda$ free space wavelength), $b=0.55\lambda$, $h=0.05\lambda$, $T_c=0.6\lambda$, $w=0.25T_c$, $\varepsilon_{r1}=1$, $\varepsilon_{r2}=2$, $\varepsilon_{r3}=2$, and plot in Fig. 3, when 35 radial waveguide modes and 70 space harmonics are employed. The tangential electric fields are identical on both sides of the interface $\rho=b$ and vanish on the both sides of the metal surface $\rho=$a, as shown in the figure, and the tangential electric and magnetic fields are continuous over the corrugation slot region. Fig. 3 shows that the boundary conditions at the interfaces are satisfied and the electromagnetic problem is solved in the right way.

The effect of the normalized corrugation width on the radiation characteristics is shown Fig. 4. From this figure, it is found that the phase constant monotonically increases on the whole as the corrugation width increases but the leakage constant goes to a maximum and decreases again as the corrugation width increases. Since a narrow corrugation width case corresponds to the periodic corrugation width perturbation of the dielectric-coated conducting cylinder, we can expect that the leakage constant will increase as corrugation width increases. Also a wide corrugation width case can be considered as a periodic comb grating perturbation of the dielectric-coated conducting cylinder. Therefore, the leakage constant decreases as corrugation width increases and finally goes to zero. In this figure, the phase constant β/k_1 approaches to 1.2254 which is that of the dielectric-coated conducting cylinder surface wave as corrugation width goes to zero. This figure shows that the values of β and α for the finite 30 periodic corrugations obtained in an average sense[11] are very well matched to those of the infinite periodic structure.

Fig. 5 shows the effect of the coated dielectric thickness $(b-a)/\lambda$ on β/k_1 and α/k_1. It can be seen from the figure that the leakage constant α goes to a maximum and decreases again as the dielectric thickness increases while the propagation constant β monotonically increases. It indicates that both radiation angle and beamwidth change as the dielectric thickness increases. Fig. 6 shows the effect of the conducting cylinder radius a/λ on the phase and leakage constant of the leaky wave. The leakage constant has rapid decrease as the cylinder radius is small, for large radius it has almost no change while the propagation constant

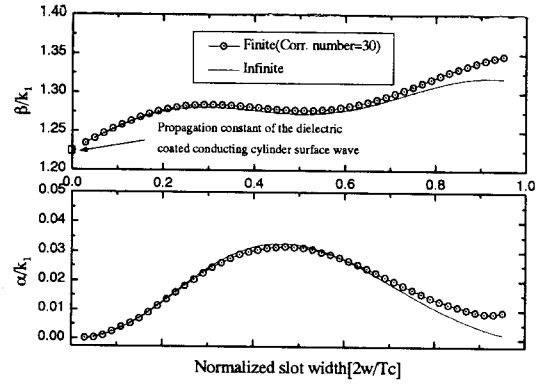

Fig. 4. Comparision of β and α between infinite and finite periodic corrugation structure with the normalized corrugation slot width as parameter: $a=0.35\lambda$, $b=0.55\lambda$, $h=0.05\lambda$, $T_c=0.6\lambda$, $\varepsilon_{r1}=1$, $\varepsilon_{r2}=2$, $\varepsilon_{r3}=2$.

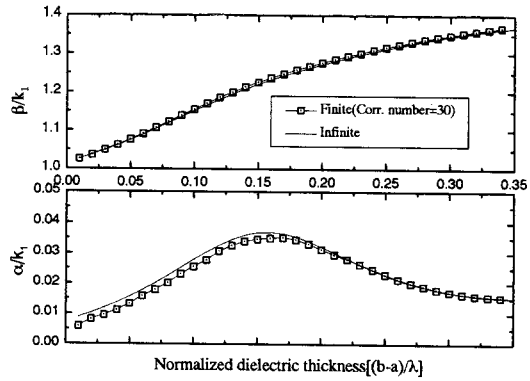

Fig. 5. Comparision of β and α between infinite and finite periodic corrugation structure with the normalized dielectric thickness as parameter: $a=0.35\lambda$, $b=0.55\lambda$, $h=0.05\lambda$, $T_c=0.6\lambda$, $\varepsilon_{r1}=1$, $\varepsilon_{r2}=2$, $\varepsilon_{r3}=2$.

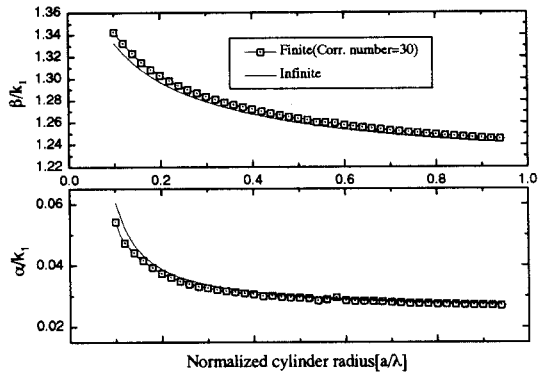

Fig. 6. Comparision of β and α between infinite and finite periodic corrugation structure with the normalized cylinder radius as parameter: $b=a+0.2\lambda$, $h=0.05\lambda$, $T_c=0.6\lambda$, $w=0.25T_c$ $\varepsilon_{r1}=1$, $\varepsilon_{r2}=2$ $\varepsilon_{r3}=2$.

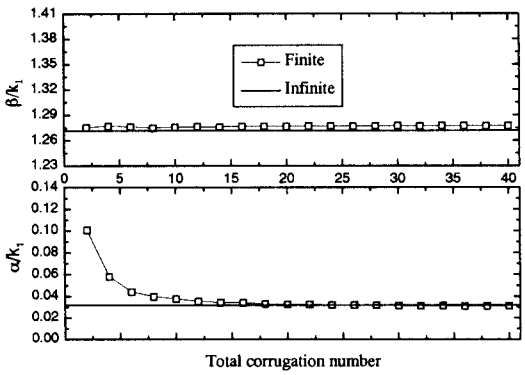

Fig. 7. Variation of β and α with total corrugation number as parameter; $a=0.35\lambda$, $b=0.55\lambda$, $h=0.05\lambda$, $T_c=0.6\lambda$, $w=0.25T_c$, $\varepsilon_{r1}=1$, $\varepsilon_{r2}=2$, $\varepsilon_{r3}=2$.

monotonically decreases. Thus we can expect that the beamwidth has almost no change but the radiation angle changes for $a>0.2\lambda$. Fig. 5 and Fig. 6 show good agreements between β and α of infinite periodic structure and those of finite periodic structure over for all parameter ranges.

The variation of the complex propagation of the finite periodic corrugations obtained in an average sense is plotted in Fig. 7 for increasing the number of the corrugation. The complex propagation

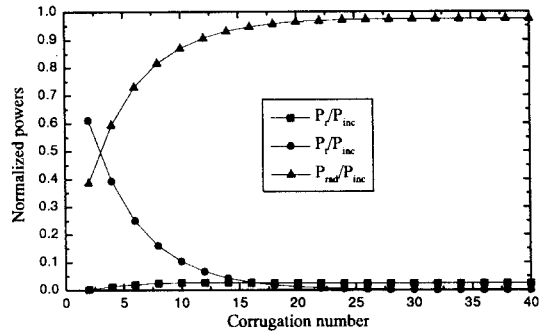

Fig. 8. Normalized power P_r, P_t, and Prad versus total conrrugation number: $a=0.35\lambda$, $b=0.55\lambda$, $h=0.05\lambda$, $T_c=0.6\lambda$, $w=0.25T_c$, $\varepsilon_{r1}=1$, $\varepsilon_{r2}=2$, $\varepsilon_{r3}=2$.

($\beta-j\alpha$) of the finite corrugations is almost the same as the one of the infinite structure when the corrugation number is larger than 20. Thus, It is expected that the radiation characteristics of the finite periodic corrugations are very well matched to those of the infinite structure, because the leaky wave main beam radiation angle is determined by β and 3 dB beamwidth of the leaky wave antenna related with α.

The variation of the powers versus the corrugation number is shown in Fig. 8. This figure shows that the power conservation law is satisfied for all corrugation numbers. The transmitted power is decreased as the corrugation number increases, while the radiated power is increased. For the case of corrugation number 40, 97.5% of the incident power is radiated, 2.5% is reflected, and the transmitted power almost vanished. Thus, when the leaky-wave mode is established in the finite structure, most of the incident power is radiated into free space.

Fig. 9 shows the radiation pattern of the finite periodic corrugations calculated by (17) compared to the results evaluated by using (7) from the study of an infinite structure. The main beam radiation angle($\theta_{-1}\approx113.2°$) and beamwidth($\theta_{0.5}\approx3.7°$) are almost the same, the directivity gain is

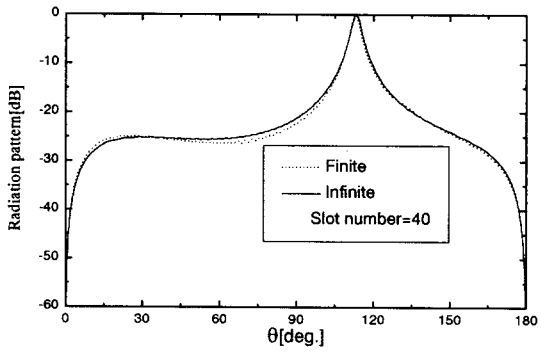

Fig. 9. Radiation pattern: $a=0.35\lambda$, $b=0.55\lambda$, $h=0.05\lambda$, $T_c=0.6\lambda$, $w=0.25T_c$, $\varepsilon_{r1}=1$, $\varepsilon_{r2}=2$, $\varepsilon_{r3}=2$.

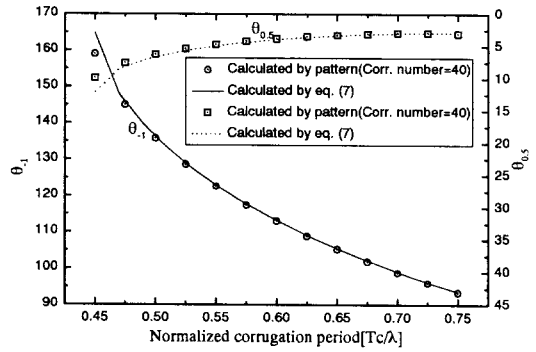

Fig. 10. Comparison of beamwidth and radiation angle between infinite and finite periodic corrugation structure with the normalized corrugation period as parameter: $a=0.35\lambda$, $b=0.55\lambda$, $h=0.05\lambda$, $w=0.25T_c$, $\varepsilon_{r1}=1$, $\varepsilon_{r2}=2$, $\varepsilon_{r3}=2$.

about 13.36 dB, but some discrepancies between finite and infinite case are observed in the side lobes. This is due to the effect of the end sections of the finite structure.

Fig. 10 shows the beam scanning characteristics of finite periodic corrugations versus normalized corrugation period. In this figure, the radiation angle θ_{-1} changes from the endfire direction to broadside as the period increases and 3 dB beamwidth decreases as the corrugation period increases. It is observed that radiation angle and beamwidth are almost same to those evaluated by using (7) from the study of an infinite structure. It should be noted that the radiated power(P_{rad}) normalized by the incident power is greater than 0.93 for $T_c \geq 0.5\lambda$. If the period is 0.45λ, the normalized reflected and radiated power(P_r and P_{rad}) is 0.25 and 0.74, respectively, thus it is a little undesirable because it decreases the efficiency of the antenna.

As may be seen from Fig. 9, the uniform finite periodic corrugation has relatively high side lobes, which reduces its utility as high-performance of the leaky wave antenna. For low side lobe and narrow beam requirements, the structure must be tapered. First, we introduce corrugation width and depth tapering process on the beginning and end section of antenna to lower side lobe level. We tapered five corrugation widths and depths to be linearly increased and decreased on the beginning and end section of antenna, respectively. Fig. 11 shows the radiation patterns with tapered section compared with those of no tapering section. It is found that the side lobe levels are lowered more than 10 dB compared to those of no tapering case, keeping the antenna efficiency.

Next, we consider the design aspect of the problem which is aimed at improvement of the radiation pattern by making use of a nonuniform

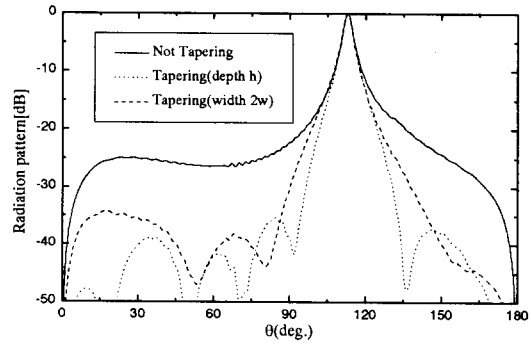

Fig. 11. Radiation pattern with reduced side lobes by corrugation width and depth tapering: $a=0.35\lambda$, $b=0.55\lambda$, $h=0.05\lambda$, $T_c=0.6\lambda$, $w=0.25T_c$, $\varepsilon_{r1}=1$, $\varepsilon_{r2}=2$, $\varepsilon_{r3}=2$.

quasi-periodic array. To this end, suppose that the minimum main beam width at given side lobe level have to be reached, i.e., let us synthesize the Taylor pattern. According to the local periodicity conception[6], the leakage rate per period and the maximum radiation angle of a leaky wave traveling along a uniform periodic array must be known as function of corrugation slot width provided that a certain period is chosen(Fig. 12). Let us side lobe level of −25 dB be desired and the main beam direction be 113°. In addition, let the array being designed contain 41 corrugation slots, and let relative transmitted power of 5% be allowable. Using the theory of the Taylor pattern

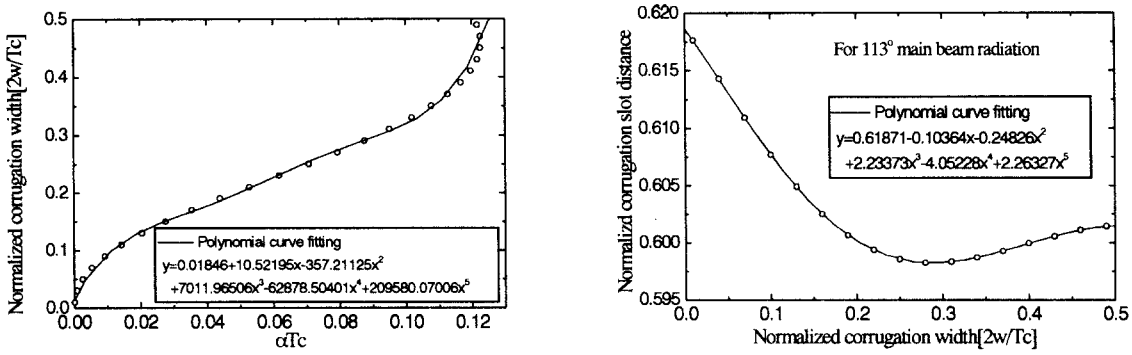

Fig. 12. Variation of the normalized corrugation slot width with the leakage rate per period and corrugation slot distance normalized by with the corrugation slot width as parameter: $a=0.35\lambda$, $b=0.55\lambda$, $h=0.05\lambda$, $T_c=0.6\lambda$, $w=0.25T_c$, $\varepsilon_{r1}=1$, $\varepsilon_{r2}=2$, $\varepsilon_{r3}=2$.

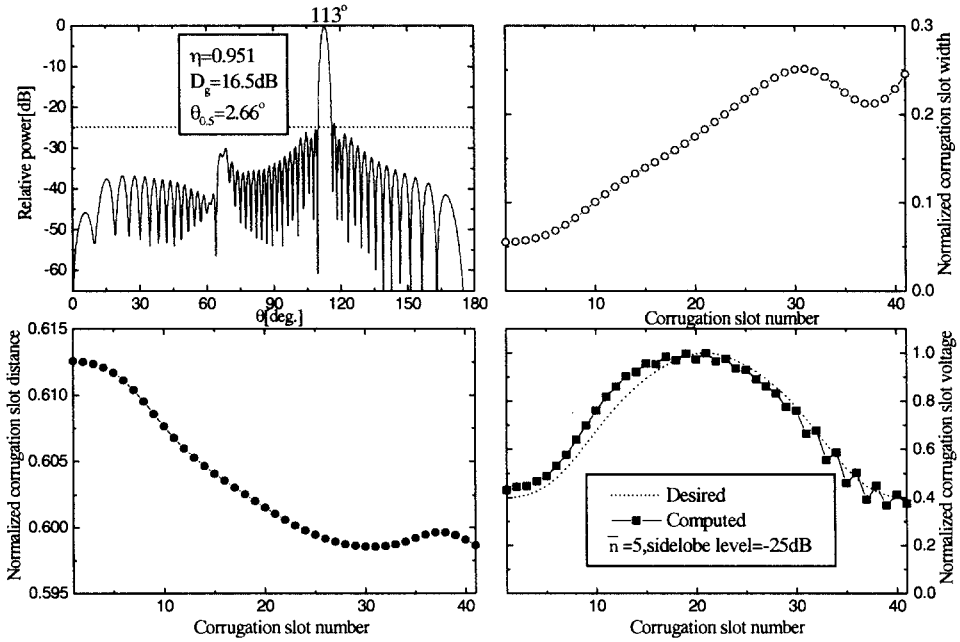

Fig. 13. Radiation pattern, slot width distribution, slot distance distribution, and slot voltage distribution of a structure producing Taylor pattern: $a=0.35\lambda$, $b=0.55\lambda$, $h=0.05\lambda$, $T_c=0.6\lambda$, $w=0.25T_c$, $\varepsilon_{r1}=1$, $\varepsilon_{r2}=2$, $\varepsilon_{r3}=2$.

for discrete arrays[12] and assuming the parameter $\overline{n}=5$, one can calculate the necessary normalized corrugation slot voltage along the array and leakage rate per period that both correspond to the desired pattern[12]. Next, using the desired voltage distribution and graph of Fig. 13, it is easy to determine necessary corrugation slot widths. In addition, taking into account the relationship between maximum radiation angle and corrugation slot width, spacing between centers of adjacent corrugation slots should be slightly changed to ensure the same radiation angle from all local periods of the array. The values of the slot widths and slot distances, thus defined, are plotted in Fig. 13. Now all the parameters of the array are completely determined. The computed and desired normalized slot voltage distributions in the array are shown in Fig. 13. This figure shows very good agreements between computed and desired ones. The computed radiation pattern is also presented in Fig. 13. As seen, the actual side lobe level and main beam radiation angle are in very good agreement with the desired values. The efficiency of the antenna is 95% and transmitted power does not exceed the specified level 5%. The directivity gain of the antenna is almost 3.15 dB larger than that of the uniform periodic corrugation slot array. Thus, it may be concluded that the design requirements are successfully fulfilled in the considered variant. The good agreement between the desired and computed values testifies the correctness of the local periodicity conception.

Especially, the finite periodic corrugation gives end-fire radiation pattern with specified corrugation period and depth, which was used in a corrugated surface wave antenna[13], but it has very high side lobe levels. To reduce side lobe levels, we introduce the corrugation width tapering process on the beginning and end section of the antenna. In the case of $a=0.35$, $b=0.5\lambda$, $T_c=0.25\lambda$, $w=0.45T_c$, $\varepsilon_{r1}=1$, $\varepsilon_{r2}=2$, $\varepsilon_{r3}=2$, with the corrugation

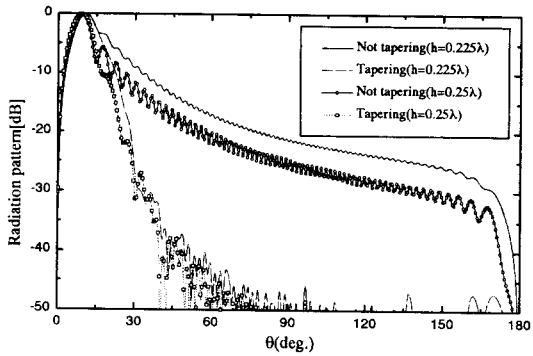

Fig. 14. Endfire radiation pattern: $a=0.35\lambda$, $b=0.55\lambda$, $T_c=0.25\lambda$, $w=0.45T_c$, $\varepsilon_{r1}=1$, $\varepsilon_{r2}=2$, $\varepsilon_{r3}=2$.

number 133, we tapered 30 corrugation widths to be linearly increased and decreased on the beginning and end section of antenna, respectively. Fig. 14 shows endfire radiation pattern having low side lobe levels more than 20 dB compared to those of no tapering case for the corrugation depth $h=0.225\lambda$, $h=0.25\lambda$, respectively.

V. Conclusion

The analysis method for the dielectric-coated conducting cylinder with infinite periodic corrugation as a leaky wave antenna, and the solution method for the leaky wave radiated from the finite periodic corrugation loaded conducting cylinder excited by the TM incident surface wave have been proposed. In this paper, rigorous mode matching was applied to obtain the complex propagation constant of the leaky wave for the corrugation case of the infinite periodic structure.

The validity of the proposed method was checked by calculating tangential electromagnetic fields at the interfaces and by applying the power conservation law. Phase and attenuation constants were calculated with corrugation slot width, corrugation depth, dielectric thickness, and cylinder radius as parameters. Also the radiation pattern of the antenna were calculated. The main beam

radiation angle and beamwidth of the finite periodic corrugation were well matched to those of the infinite structures except for the side lobes due to the finite end effect. A good agreement between the results of the finite periodic structures and those of infinite structures has been found. The variations of the complex propagation constant of the finite periodic corrugation were calculated for increasing corrugation slot numbers and good agreement compared with infinite periodic corrugation were obtained for more than the total 20 numbers. Also the powers(reflected, transmitted and radiated powers) of the finite periodic corrugation were calculated for increasing corrugation slot numbers and most of the incident power was radiated into free space for more than the total 20 numbers. The uniform finite periodic corrugation has relatively high side lobes. For reduced side lobes and narrow beam requirements, through tapering process of the beginning and end section of the antennas, we obtained the radiation pattern with reduced side lobes. Also to accomplish that the minimum main beam width at given side lobe level have to be reached, we synthesized Taylor pattern. For finding a solution to this problem, a combination of the proposed approach together with the local periodicity conception assuming quasi-periodicity was used here. We obtained Taylor pattern to produce the desired radiation pattern.

Especially, for the specified corrugation period, width and depth used in a corrugated surface wave antenna design, through the proper tapering process, we obtained end-fire radiation pattern with reduced side lobe levels. The proposed methods in this paper are helpful to predicting the performance of the leaky wave antenna at the design stage.

References

[1] J. Jacobsen, "Analytical, numerical, and experimental investigation of guided waves on periodically strip-loaded dielectric slab," *IEEE Trans. Antennas Propagat.*, vol. 18, no. 3, pp. 379-388, May, 1970.

[2] T. Itoh, "Application of gratings in a dielectric waveguide for leaky wave antennas and band-reject filters," *IEEE Trans. Microwave Theory Tech.*, vol. MTT-25, pp. 1134-1138, Dec., 1977.

[3] M. Matsumoto, M. Tsutsumi, and N. Kumagai, "Radiation characteristics of a dielectric slab waveguide periodically loaded with thick metal strips," *IEEE Trans. Microwave Theory Tech.*, vol. MTT-35, pp. 89-95, Feb., 1987.

[4] J. A. Encinar, "Mode-matching and point-matching thechniques applied to the analysis of metal-strip-loaded dielectric antennas," *IEEE Trans. Antennas Propagat.*, vol. 38, pp. 1405-1412, Sept., 1990.

[5] K. Uchida, "Numerical analysis of surface-wave scattering by finite periodic notches in ground plane," *IEEE Trans. Microwave Theory Tech.*, vol. 35, no. 5, pp. 481-486, May, 1987.

[6] V. I. Kalinichev, "Diffraction characteristics of a finite metal-strip grating integrated with a planar dielectric waveguide," *IEICE Trans. Electron.*, vol. E78-C, no. 10, pp. 1447-1452, Oct., 1995.

[7] J. P. Kim, C. W. Lee, and H. Son, "Leaky wave radiation from dielectric-coated parallel-plate waveguide periodic slot with finite thickness," *The Journal of Korea Electromagnetic Engineering Society*, vol. 10, no. 2, pp. 247-256, Apr., 1999.

[8] S. Xu, J. Min, S. T. Peng, F. K. Schwering,

"A millimeter-wave omnidirectional circular dielectric rod grating antenna," *IEEE Trans. Antennas Propagat.*, vol. 39, no. 7, pp. 883-891, July, 1991.

[9] S. Xu, and X. Wu, "A millimeter-wave omnidirectional dielectric rod metallic grating antenna," *IEEE Trans. Antennas Propagat.*, vol. 44, no. 1, pp. 74-79, Jan., 1996.

[10] C. W. Lee, and H. Son, "Radiation characteristics of dielectric coated coaxial waveguide periodic slot with finite and zero thickness," *IEEE Trans. Antennas Propagat.*, vol. 47, no. 1, pp. 16-25, Jan., 1999.

[11] C. W. Lee, and H. Son, "Periodically slotted dielectrically filled parallel-plate waveguide as a leaky wave antenna : E-polarization case," *IEEE Trans. Antennas Propagat.*, vol. 47, no. 1, pp. 171-178, Jan., 1999.

[12] C. A. Balanis, *Antenna Theory*, John Wiley Sons, New York, 1982.

[13] J. P. Kim, C. W. Lee and H. Son, "Analysis of corrugated surface wave antenna using hybrid MOM/UTD technique," *Electron. Lett.*, vol. 35, no. 5, pp. 353-354, March, 1999.

김 중 표

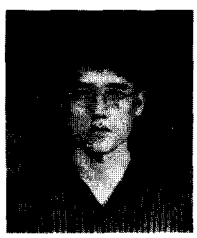

1991년 2월: 경북대학교 전자공학과(공학사)
1993년 2월: 경북대학교 대학원 전자공학과(공학석사)
1993년 3월~2000년 2월: 경북대학교 대학원 전자공학과(공학박사)
2003년 3월~현재: 한국 항공우주연구소 선임연구원
[주 관심분야] 전자파 산란 및 수치해석, 안테나 설계 및 해석

손 현

1960년 8월: 연세대학교 전기공학과(공학사)
1975년 8월: 한양대학교 대학원 통신공학과(공학석사)
1984년 8월: 경희대학교 대학원 전자공학과(공학박사)
1966년 4월~1977년 4월: 주한 미 육군 정보통신단 작전과 기술지원실 기술부장
1977년 4월~현재: 경북대학교 전자공학과 교수
[주 관심분야] 이동통신, 위성통신, 마이크로파 및 안테나